A coupled numerical–experimental approach for bender-based G_0 measurements in geomaterials

Un couplage numérique-experimentale pour la mesure de G_0 avec Bender Elements dans Geomateriaux

Ionut Dragos Moldovan
CERIS, ICIST, Instituto Superior Técnico, University of Lisbon, Portugal, dragos.moldovan@tecnico.ulisboa.pt

António Gomes Correia, Cláudio Pereira
Institute for Sustainability and Innovation in Structural Engineering (ISISE), School of Engineering, University of Minho, Guimarães, Portugal

ABSTRACT: Bender elements are shear wave transducers, used for the experimental identification of the small-strain shear moduli of geomaterials. They offer good coupling with the sample and controllable loading signal and frequency, but the interpretation of their readings poses considerable difficulties. This study lays the foundations for a coupled, numerical–experimental approach to this issue, using hybrid-Trefftz finite elements to model the bender element experiment. Two main reasons justify the choice of these elements. First, they are much less wavelength-sensitive than conventional finite elements, meaning that coarse meshes can be used to model waves of very different types and frequencies. Second, hybrid-Trefftz elements use physically meaningful approximation bases. This enables the numerical filtration of the spurious waves from the response of the sample. The elements recover adequately the output signal obtained experimentally, for multiple laboratorial setups. The numerical filtration of the compression waves endorses the clear identification of the shear wave arrival.

RÉSUMÉ : Les Bender Elements sont des transducteurs de mesure de propagation d'ondes de cisaillement utilisés pour l'identification expérimentale des modules de cisaillement en petites déformations des géomatériaux. Ils offrent un bon couplage avec l'échantillon et le signal de chargement contrôlable et la fréquence, mais l'interprétation de leurs lectures pose des difficultés considérables. Cette étude établi les bases d'une approche numérique – expérimentale couplée à cette question, à l'aide des éléments finis hybride-Trefftz pour modéliser l'expérience avec Bender Elements. Deux raisons principales justifient le choix de ces éléments. Tout d'abord, ils sont beaucoup moins sensibles à la longueur d'onde que les éléments finis classiques, ce qui signifie que de maillages grossiers peuvent servir à la modélisation des ondes de diffèrent types et fréquences. D'autre part, les éléments hybride-Trefftz utilisent bases de rapprochement physique. Cela permet le filtrage numérique des ondes parasites de la réponse de l'échantillon. Les éléments récupèrent correctement le signal de sortie obtenu expérimentalement, pour plusieurs configurations de laboratoires. Le filtrage numérique des ondes de compression permet l'identification claire de l'arrivée d'ondes de cisaillement.

KEYWORDS: small strain shear modulus, bender element test, hybrid-Trefftz finite element.

1 INTRODUCTION

Bender elements were introduced for measuring the shear wave velocity in geomaterials in 1978 (Shirley 1978). Their effectiveness was confirmed in various studies, e.g. (Dyvik and Madshus 1985), but their use in the industry is hampered by the difficulties regarding the interpretation of the output signal. In a typical setup, two bender elements are used: one generates the shear wave (the emitter) and the other reads it at some other end of the sample (the receiver). The arrival time of the wave gives its velocity, which is used to obtain the shear modulus. However, the definition of the arrival time is not simple, as the induced shear wave suffers multiple reflections and distortions while it travels through the sample and is further polluted by the compressional waves triggered by the lateral motion of the emitter (Brignoli, Gotti and Stokoe 1996). Many classes of approaches, ranging from visual observation to complex signal analysis, were suggested for the identification of the arrival time (Lee and Santamarina 2005), with no apparent consensus. One problem is that most signal interpretation techniques are based on knowledge of the input and output signals alone, and ignore what goes on between the input and output readings.

Significant insight into the wave propagation could be gained from the numerical simulation of the bender element experiment. A numerical model, preferably considering the multi-phase nature of geomaterials, would describe in detail the wave propagation and expose the wave distortion caused by spurious reflections from the lateral boundaries of the sample.

Despite such prospects, few studies report on the numerical modelling of bender element experiments. The available models are based either on the finite element method (Johnson 2008), finite difference method (Arroyo, et al. 2006), or discrete element method (O'Donovan, O'Sullivan and Merketos 2012). The main issue hindering all numerical approaches is the high frequencies involved in the testing, which require very small time steps in transient analyses, and extremely refined meshes. Direct comparison of the modelled and recorded output signals is very rare and the success has been generally limited (Johnson 2008). Recently, a series of papers reported on the development of hybrid-Trefftz finite elements for multi-phase materials (e.g. (Moldovan and Freitas 2012)). Trefftz elements use domain approximations that satisfy exactly the differential equation governing the problem. Consequently, the elements are wavelength-insensitive and distinguish naturally between the various types of waves present in the response of the sample. The former feature renders hybrid-Trefftz elements ideally suited for modelling high frequency transient problems, while the latter enables the numerical filtration of certain types of waves (compression or shear) from the response of the sample.

The objective of this paper is to show how the favourable features of the hybrid-Trefftz elements can be used to improve the output signal interpretation in bender element experiments. The descriptions of the experimental and numerical setups are followed by the validation of the results obtained using the

numerical simulation against the output signals obtained experimentally. Two strategies for improving the interpretation of the output signal by harvesting information from the numerical model are then suggested. A more complete version of this study is presented in (Moldovan, Gomes Correia and Pereira 2016).

2 EXPERIMENTAL SETUP

In 2003, an international parallel test on the measurement of small strain shear moduli was launched by the International Society of Soil Mechanics and Geotechnical Engineering. Its objective was to assess the consistency of the G_0 measurement using bender elements (Yamashita, et al. 2009). Samples of the same material (a Toyoura sand) were shipped to 23 laboratories in 11 countries and the shear modulus was measured on each sample. The laboratories could choose the experimental setup according to their preference. By 2006, the measurements were concluded and vast differences in the measured shear moduli were reported. An especially tricky situation was that of a dry material with low or null confining pressure, where the average shear modulus was less than twice the standard deviation. This challenging situation is used in all tests reported in this work.

1 .1 *Equipment*

The bender element apparatus involves two (transmitter and receiver) bender elements embedded in standard inserts (Figure 1(a)). The elements are 11mm in width, 1.8mm in thickness 7mm in length (all dimensions include the epoxy coating).

The bender elements are installed in a cylindrical mould filled with Toyoura sand. The mould is made of an acrylic material 6.5mm thick and has the height of 200mm and the internal diameter of 100mm. The size of the sample is chosen to ensure that the distance between the emitter and receiver bender elements is larger than twice the wavelength, for the lowest frequency tested, to mitigate the near-field effect in the readings (Arroyo, et al. 2006). The emitter element is embedded in the centre of an aluminium platen, as shown in Figure 1(b), and fixed to the mould. The receiver element is located at the upper surface of the sample, precisely above the emitter. The top surface of the sample is open and the receiver is inserted using an external steel structure (Figure 2). Note that a closed top surface was also tested and the results published in (Moldovan, Gomes Correia and Pereira 2016). Since the results were largely similar, only the open surface setup is reported here, because of space limitations.

The experiments are performed using harmonic pulse excitations of 1, 2, 3 and 4kHz frequency, which include the range where the resonant frequency of the coupled bender element-soil system is expected to lay.

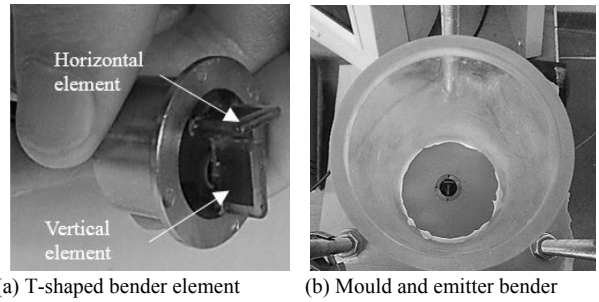

(a) T-shaped bender element (b) Mould and emitter bender element

Figure 1. Bender element equipment.

1 .2 *Material*

Classified as a monogranular or poorly-graded material, the Toyoura sand is used in the tests reported in this work. Its physical properties are given in Table 1 and the grain size distribution curve is shown in Figure 3. The specimens were prepared using the dry tamping method. The material was left to dry in an oven for 24h to remove eventual initial moisture.

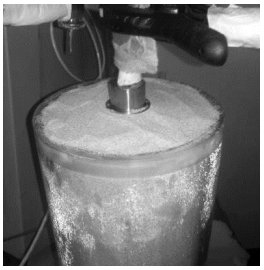

Figure 2. Receiver bender element inserted in the specimen.

Table 1. Physical properties of Toyoura sand.

Property	Value
Specific gravity	2.65
Maximum void ratio	0.928
Minimum void ratio	0.677
Mean grain size, D_{50} (mm)	0.15
Coefficient of uniformity	1.43

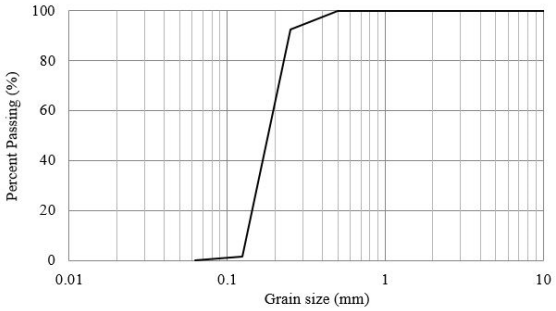

Figure 3. Grain size distributions of the Toyoura sand.

3 NUMERICAL SETUP

The numerical model used to simulate the wave propagation through the sample of Toyoura sand is constructed using the displacement model of the hybrid-Trefftz finite elements (Moldovan and Freitas 2012). It is based on the well-known Biot's theory of porous media (Biot 1956) and treats the material as a porous medium saturated with air. The simplifying assumptions and mathematical formulation of the model are presented in detail in (Moldovan, Gomes Correia and Pereira 2016) and are not restated here.

As opposed to conforming displacement (conventional) finite elements, the approximation bases of the hybrid-Trefftz elements are specifically tailored for each problem they solve. Each shape function designates a type of wave whose contribution to the structural response is calculated such as to recover, in the best possible way, the initial and boundary conditions. The physical information built into the Trefftz basis enhances the convergence of the elements and renders them insensitive to issues known to hinder the performance of conventional finite elements, like gross mesh distortion, incompressible constituents, and large wavelength variations (Moldovan and Freitas 2012). Consequently, coarse finite element meshes can be used for a very wide range of excitation frequencies, without the need to calibrate the element size to the

wavelength content. Moreover, since the shape functions are actual wave types, the filtering of the spurious waves from the response of the sample is rather straightforward.

The numerical model uses a (very coarse) mesh of 66 hybrid-Trefftz finite elements to discretize the sample, as presented in Figure 4. In each element, 81 (Bessel type) shape functions are used to approximate the displacement and air seepage fields, and 24 (polynomial) shape functions are used on each Dirichlet and interior boundary to approximate the tractions in the solid phase and the pore pressure. The total number of degrees of freedom for the model is 8574.

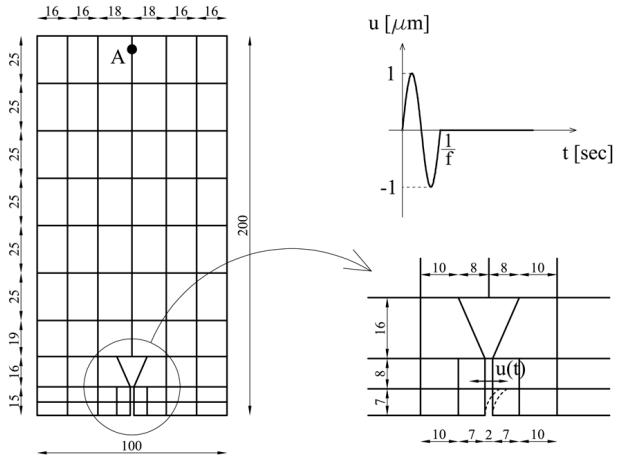

Figure 4. Finite element mesh and input signal (dimensions in mm).

Except for the upper surface of the mould, all exterior boundaries are defined as Dirichlet. Null normal displacement and air seepage are enforced on the boundaries, except for the two long sides of the emitter bender element, where the normal displacements are designed to reproduce its lateral motion. A cantilever displacement of $1.0\mu m$ amplitude is enforced at that location (Figure 4). All boundaries are considered frictionless. The upper surface of the mould is defined as a Neumann boundary with null tractions and pore pressures.

A single time step is used for the analysis of the wave propagation over an interval of 5.0msec. The time basis is constructed using 128 Daubechies wavelet and scale functions, with a resolution level of 5. The displacement time-history is recorded at point A(50,193)mm (Figure 4), corresponding to the tip of the receiver bender element. However, the receiver is not explicitly included in the model.

4 VALIDATION

The numerical model described in Section 3 is validated by direct comparison between the experimental output signal and the simulated time-history of the horizontal displacement at point A (Figure 4).

The overlapping between the experimental and simulated output signals is presented in Figure 5, for the four tested input frequencies. The left vertical axis (associated to the grey line) measures the intensity of the output signal recorded by the receiver. The right vertical axis (associated to the black line) measures the displacement at point A normalized to the amplitude of the displacement of the tip of the emitter. For all tested frequencies, the computational model recovers well the features of the recorded signal until after the largest displacement peaks in the plots. These peaks are due to the rebound of the main shear wave from the top of the sample, which doubles the effect of the inbound wave near that boundary. After this, the correspondence between the measured and simulated signals is compromised since the receiver bender element is not included in the model. Because of the significant impedance discrepancy between the sample and the receiver, the presence of the receiver element influences considerably the shear wave rebound. This issue does not interfere, however, with the ability of the numerical model to identify the first arrival of the shear wave, since its predictions only deteriorate after the reflection of that wave from the top surface.

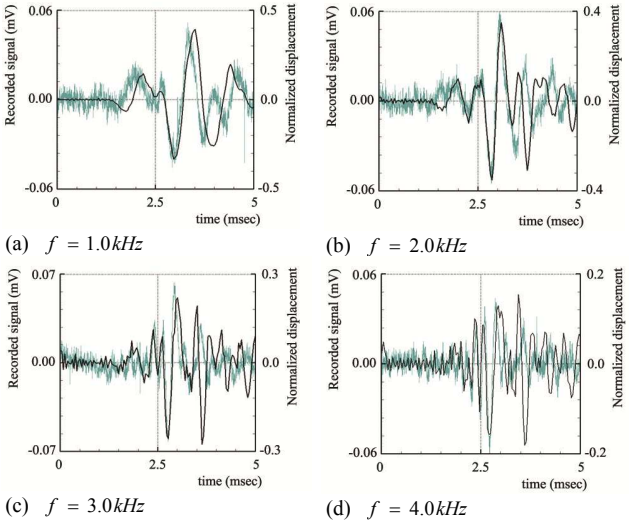

Figure 5. Displacement time-histories at point A(50,193)mm, recorded experimentally (grey line) and simulated numerically (black line).

In all plots, the arrival of the waves at the receiver present three key zones. The first zone corresponds to the first significant peaks, roughly between 1.5 and 2.0msec. The second key region is near 2.5msec, where oscillations of higher amplitude form either a plateau region (Figure 5(b)) or an M-shaped pattern (Figures 5(c) and 5(d)). This region is less visible in the lower amplitude case (Figure 5(a)). Finally, the reflection of the main wave front from the top surface is characterized by a single, high amplitude oscillation in all plots. The arrival of the shear wave occurs at some point in the first two of the regions described above. However, by simple observation of the experimental output signal, it is unlikely that the arrival time can be clearly pinpointed.

5 FIRST ARRIVAL IDENTIFICATION

Two alternative approaches for the unequivocal identification of the shear wave arrival are described next, based on the additional information gathered from the numerical model. The procedures are described using the 3.0kHz excitation frequency.

5 .1 *First arrival identification using wave propagation plots*

The simplest approach to the identification of the arrival time of the shear wave is by the direct observation of the horizontal displacement fields that occur throughout the sample at it propagates. To illustrate this strategy, consider the time-history of the horizontal displacements at point A (black line in Figure 5(c)), on the time interval where the shear wave arrival is expected to occur (Figure 6). Four amplitudes are marked in Figure 6, each possibly corresponding to the arrival of the shear wave. The horizontal displacement fields in the whole sample are plotted as colour maps at these four time points in Figure 7. The plots are made on the deformed shape of the sample, to endorse the direct observation of the enforced boundary conditions and of the Rayleigh wave at the free surface.

As a general note, the displacement fields recover without visible flaws the inter-element continuity and the applied boundary conditions (hybrid-Trefftz elements enforce boundary conformity in a weak form, thus the observation of this conditions is not trivial). The observation of the plots also

reveal the propagating shear wave and endorse the clear identification of its arrival at the receiver. At $t_1 = 1.84$msec, the shear wave front is still rather far from the upper surface of the sample, so the perturbations recorded in the first region described in Section 4 are caused by compression wave fronts reflected from the lateral boundaries of the sample and propagating with velocities superior to that of the shear wave. Their propagation is characterized by a cross pattern, with multiple reflections, which explains the time spreading of these perturbations. Conversely, the second large peak in the displacement time-history corresponds to the arrival of the shear wave at the receiver, as visible in Figure 7(b). This amplitude is immediately followed by another (Figure 7(c)), forming the arrival pattern in the shape of an M. Subsequently, the shear wave arrives at the top of the sample and bounces back, causing the largest displacement amplitudes, as visible in Figure 7(d). It should be noted that the largest peaks in the receiver's reading do not correspond to the arrival of the shear wave, but to its reflection from the top of the sample.

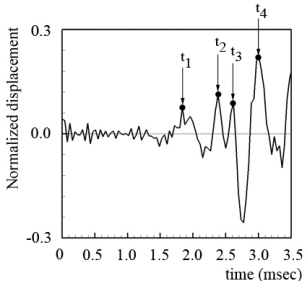

Figure 6. Selected instants for the displacement field representation.

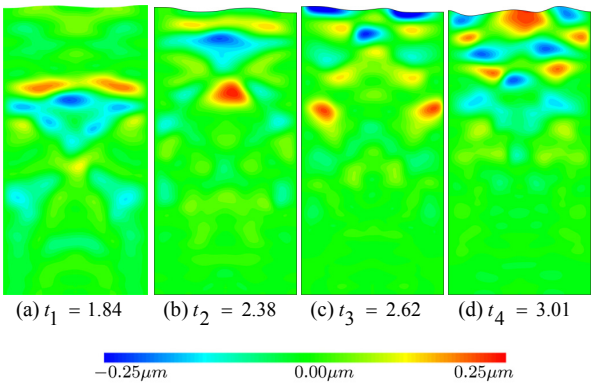

Figure 7. Horizontal displacement plots at selected instants.

5 .2 *First arrival identification by modal decomposition*

While the arrival time of the main shear wave is simple to grasp by just observing the horizontal displacement plots, as shown in the previous section, it may be pinpointed with more precision by uncoupling the compression and shear waves (modes) in the response of the sample. The procedure is grounded in the trademark feature of the hybrid-Trefftz elements of distinguishing naturally between compression and shear wave components, and does not require the repetition of the analysis. To illustrate the process, the time-histories of the (normalized) horizontal displacements at point A, obtained by considering only the compression modes and only the shear modes, are presented in Figure 8(a) and (b), respectively. For comparison, the full signal is plotted (in black) in Figure 5(c).

Around $t = 1.5$msec, the first compression waves arrive at the receiver, immediately followed by spurious shear waves produced by the mode conversion phenomenon after the reflection of the compression waves from the lateral envelope of the sample. The arrival of the main shear wave produces the M-shaped horizontal displacement pattern visible in Figure 5(c). This is quite problematic from the signal interpretation perspective, since it may be unclear if the arrival time corresponds to the first amplitude, second amplitude or it lays somewhere in-between. Conversely, the filtration of the compressional waves from the displacement time-history (Figure 8(b)) enables the clear identification of the first shear amplitude at $t = 2.38$msec. The amplitude of the shear-only normalized displacement at this point is $u = 0.155$, considerably superior to that obtained by including all types of waves ($u = 0.113$, in Figure 5(c)). This means that the compression waves conceal, to some extent, the arrival of the shear wave. The opposite is true at the second displacement peak, at $t = 2.62$msec. Of the total normalized displacement of $u = 0.089$ (Figure 5(c)), only half is caused by shear waves (Figure 8(b)), while the rest is contributed by the compression waves (Figure 8(a)).

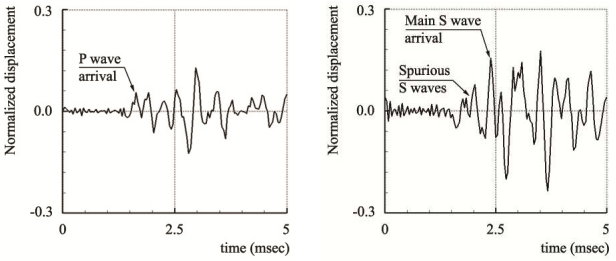

(a) Compression waves (b) Shear waves

Figure 8. Modal decomposition of the time-history at point A.

6 ACKNOWLEDGEMENTS

This research was supported by Fundação para a Ciência e a Tecnologia through project PTDC/ECM/122751/2010 and grant SFRH/BPD/87317/2012, and by the European Union through project FCOMP-01-0124-FEDER-020365.

7 REFERENCES

Arroyo, M., Muir Wood, D., Greening, P. D., Medina, L., and Rio, J. 2006. Effects of sample size on bender-based axial G0 measurements. *Géotechnique* 56 (1), 39-52.

Biot, M. A. 1956. Theory of propagation of elastic waves in a fluid saturated porous solid. II. High frequency range. *Journal of the Acoustical Society of America* 28 (2), 179-191.

Brignoli, E. G., Gotti, M., and Stokoe, K. H. 1996. Measurement of Shear Waves in Laboratory Specimens by Means of Piezoelectric Transducers. *Geotechnical Testing Journal* 19 (4), 384–397.

Dyvik, R., and Madshus, C. 1985. Lab measurements of Gmax using bender element. *ASCE Convention on Advances in the Art of Testing Soils under Cyclic Conditions*, 186-196.

Johnson, S. 2008. *Modeling a Bender Element Test using Abaqus Finite Element Program.* Cambridge, MA: Massachusetts Institute of Technology.

Lee, J.-S., and Santamarina, J. 2005. Bender Elements: Performance and Signal Interpretation. *Journal of Geotechnical and Geoenvironmental Engineering* 131 (9), 1063-1070.

Moldovan, I. D., and Freitas, J. A. 2012. Hybrid-Trefftz displacement and stress elements for bounded poroelasticity problems. *Computers and Geotechnics* 42, 129-144.

Moldovan, I. D., Gomes Correia, A., and Pereira, C. 2016. Bender-based G0 measurements: a coupled numerical-experimental approach. *Computers and Geotechnics* 73, 24-36.

O'Donovan, J., O'Sullivan, C., and Merketos, G. 2012. Two-dimensional discrete element modelling of bender element tests on an idealised granular material. *Granular Matter* 14, 733–747.

Shirley, D. J. 1978. An improved shear wave transducer. *Journal of the Acoustical Society of America* 63(5), 1643–1645.

Yamashita, S., Kawaguchi, T., Nakata, Y. M., Fujiwara, T., and Shibuya, S. (2009). International parallel test on the measurement of Gmax using bender elements. *Soils and Foundations* 49(4), 631-650.